

## Quantifying polaronic effects on the scattering and mobility of charge carriers in lead halide perovskites

Lewis A. D. Irvine , Alison B. Walker , and Matthew J. Wolf \*

*Department of Physics, University of Bath, Claverton Down, Bath BA2 7AY, United Kingdom*

 (Received 28 May 2020; revised 7 April 2021; accepted 27 May 2021; published 25 June 2021)

The formation of polarons due to the interaction between charge carriers and lattice ions has been proposed to have wide-ranging effects on charge carrier dynamics in lead halide perovskites. The hypothesis underlying many of those proposals is that charge carriers are ‘protected’ from scattering by their incorporation into large polarons. Following the approach of Kadanoff for scattering due to polar optical phonons, we derive expressions for the rates of scattering of polarons by acoustic phonons and ionized impurities, and compute the energy and angular dependent rates for electrons and holes in MAPbI<sub>3</sub>, MAPbBr<sub>3</sub>, and CsPbI<sub>3</sub>. We then use the ensemble Monte Carlo method to compute polaron distribution functions which satisfy a Boltzmann transport equation incorporating the same three scattering mechanisms, from which we extract mobilities for temperatures in the range 50–500 K. A comparison of the results with those of analogous calculations for bare band carriers indicates that polaronic effects on the scattering and mobilities of charge carriers in lead halide perovskites are more limited than has been suggested in some parts of the recent literature.

DOI: [10.1103/PhysRevB.103.L220305](https://doi.org/10.1103/PhysRevB.103.L220305)

Lead halide perovskites (LHPs) are currently the subject of intense research, primarily due to their application as an active layer in next generation semiconductor devices and photovoltaic cells in particular [1]. However, a number of fundamental aspects of their (opto)electronic properties remain under debate, such as the origins of the observed long carrier lifetimes, the seemingly benign nature of defects, and the mobility limiting scattering mechanism(s) [2,3].

In materials with polar bonding, such as LHPs, the electrostatic interaction between a charge carrier and the lattice ions in its vicinity causes the latter to be displaced from their equilibrium positions. The charge carrier and the polarized region of the lattice which surrounds it together comprise a quasiparticle known as a polaron, and polaronic effects have been suggested to play a central role in numerous elementary processes underlying charge-carrier dynamics in LHPs [4–7], including exciton dissociation [8–11], hot carrier cooling [12–17], radiative and nonradiative recombination [18–24], and steady state mobilities [18,25,26].

It is important to note the distinction between the so-called ‘small’ and ‘large’ polaron. In the former case, the charge carrier is self trapped and moves through the lattice via thermally activated hops, leading to mobilities which *increase* with temperature; in contrast, the latter is an itinerant species, exhibiting mobilities which *decrease* with temperature [27,28]. The latter scenario is consistent with experimental measurements of charge-carrier mobilities in LHPs [3,29], and it is therefore the species considered herein.

The most widely recognized consequence of large polaron formation is an increase in the effective mass of a charge

carrier from that predicted by conventional band theory. In LHPs, the increase has been calculated to be of the order of 30–70% [25,30–32] at room temperature. On the other hand, the hypothesis underlying many of the proposals of ways in which polaron formation influences charge carrier dynamics is that charge carriers are ‘protected’ from interactions with phonons, defects, and other charge carriers by their incorporation into polarons [4].

The aim of this Letter is to provide a quantitative analysis of that hypothesis, building primarily on the canonical theory of (what are now commonly known as) large polarons [33–36]. Scattering rates of polarons by acoustic phonons and ionized impurities are derived, and their values, along with those for scattering by polar-optical phonons, are computed for electron and hole polarons in MAPbI<sub>3</sub>, MAPbBr<sub>3</sub>, and CsPbI<sub>3</sub> (where MA stands for methylammonium, CH<sub>3</sub>NH<sub>3</sub>). The rates, along with the computed polaron masses, are then used to define an augmented form of Kadanoff’s semiclassical Boltzmann transport equation for polarons under the influence of a constant electric field [35,37]. Finally, the Boltzmann transport equation is solved for a range of temperatures using the ensemble Monte Carlo method [38], and the drift velocities calculated from the steady state distribution functions are used to determine temperature dependent carrier mobilities. A comparison of the results of those computations with the results of analogous calculations for bare band carriers suggests that polaron formation has a much less significant impact on carrier scattering and mobilities than has been suggested. Due to the qualitative similarity between the results for both electrons and holes in the three materials, data for electrons in MAPbI<sub>3</sub> only are presented here, and the rest of the data are provided in the Supplemental Material [39].

The simplest model of an electron in a crystalline semiconductor is that defined by the effective

\*m.j.wolf@bath.ac.uk

mass Hamiltonian:

$$H_0 = \frac{\hbar^2 |\mathbf{k}|^2}{2m^*}. \quad (1)$$

In the remainder of the paper, particles described by Eq. (1) are referred to as ‘bare band’ or simply ‘band’ electrons.

In the Feynman model of a polaron, a second particle is coupled via an harmonic potential to the electron, representing the effects of the ‘cloud of virtual phonons’ associated with the polarized region of the lattice surrounding it [33], so that the Hamiltonian takes the following form [35,37]:

$$H_F = \frac{\hbar^2 |\mathbf{k}|^2}{2m^*} + \frac{\hbar^2 |\mathbf{k}_c|^2}{2m_c} + \frac{1}{2} \kappa (\mathbf{r} - \mathbf{r}_c)^2$$

$$= \frac{\hbar^2 |\mathbf{K}|^2}{2M} + \hbar \omega_{\text{osc}} \sum_{i=1}^3 \left( (a_{\text{osc}})_i^\dagger (a_{\text{osc}})_i + \frac{1}{2} \right). \quad (2)$$

In Eqs. (1) and (2),  $\mathbf{r}$ ,  $\mathbf{k}$ , and  $m^*$  are the position, wave vector, and effective mass of the electron, with analogous quantities for the phonon cloud being identified with a ‘c’ subscript, and  $\kappa$  is the spring constant of the harmonic potential.  $M$  and  $\mathbf{K}$  are the total mass and wave vector of the polaron,  $(a_{\text{osc}})_i^\dagger$  and  $(a_{\text{osc}})_i$  are the ladder operators for the polaron’s internal harmonic oscillator state, with the index  $i$  labeling the three Cartesian directions, and  $\omega_{\text{osc}}$  is the angular frequency of the harmonic oscillator.

Despite the simplicity of the Feynman Hamiltonian, its description of large polaron dispersion relations has been shown to compare very well with the results of diagrammatic Monte Carlo calculations over a wide range of coupling strengths [43]. Furthermore, we note that it contains essential physics that commonly used electronic structure methods, such as density functional theory, do not, despite recent developments [44,45]. In particular, the degrees of freedom of the ionic cores—the quantized vibrations of which constitute phonons—are treated classically in DFT calculations, whereas the electron and the phonon cloud are treated on an equal quantum mechanical footing in Eq. (2).

The eigenfunctions of the Feynman Hamiltonian have the form of a plane wave in the center-of-mass coordinates, multiplied by a three-dimensional harmonic oscillator state in the relative coordinates, and thus describe delocalized itinerant states of a composite particle. We use the notation  $|\mathbf{K}, \mathbf{n}\rangle$  for the eigenstates, where  $\mathbf{K}$  is the polaron wave vector and  $\mathbf{n} = (n_x, n_y, n_z)$  labels the polaron’s internal oscillator state.

Equation (2) contains two free parameters, which we choose to be the total polaron mass  $M$  and the oscillator frequency  $\omega_{\text{osc}}$ . Following previous theoretical studies on large polarons in LHPs [25,30], we determine their values as functions of the lattice temperature by minimizing the expression for the free energy derived by Y. Osaka [34]. The derivation of that expression assumes the presence of a single optical phonon branch, while the real phonon band structure consists of numerous branches. In order to circumvent that problem, we follow Frost [30] in using a single effective optical phonon angular frequency  $\omega_{\text{pop}}$ , which is derived from the full optical phonon spectrum via the ‘B’ scheme of Hellwarth and Biaggio [46].

TABLE I. Material parameters for (electrons in) MAPbI<sub>3</sub> that were used in our study. Parameters were chosen to align with comparable previous studies, and sourced entirely from *ab initio* calculations reported in the literature. The elastic constant  $c_L$  was calculated from the mean value of  $C_{11}$ ,  $C_{22}$  and  $C_{33}$  presented in Ref. [40]).

Parameter	Value
Band effective mass	$m^* = 0.15m_c$ [41]
Polar optical phonon frequency	$\omega_{\text{pop}}/2\pi = 2.25$ THz [30]
Low frequency permittivity	$\epsilon_{\text{LF}} = 25.7\epsilon_0$ [41]
High frequency permittivity	$\epsilon_{\text{HF}} = 4.5\epsilon_0$ [42]
Acoustic deformation potential	$\Xi = -2.13$ eV [40]
Elastic constant	$c_L = 32$ GPa [40]

The results of minimizing the electron-polaron free energy, using the material parameters for MAPbI<sub>3</sub> contained in Table I, are presented in Fig. 1(a); they are essentially identical to those presented in Ref. [30], although there is a small discrepancy due to the conduction and valence band effective masses being swapped in that paper. The temperature dependent mass of the polaron,  $M$ , has a maximum value of  $\sim 2.3m^*$ , which it assumes at  $\sim 35$  K. However, it decreases monotonically for temperatures above that value, such that at 300 K it is only  $\sim 1.4m^*$ . We also note that the angular frequency of the polaron harmonic oscillator  $\omega_{\text{osc}}$  increases quasilinearly with temperature above  $\sim 15$  K, which results in the equilibrium probability of a polaron being in its internal ground state  $\mathbf{n} = \mathbf{0}$  being essentially independent of temperature. The probability for an electron polaron in MAPbI<sub>3</sub> is plotted in Fig. 1(b), from which it can be seen that its value remains greater than 99.7% up to a temperature of 500 K; this result has significant implications for the scattering rates of the polaron, which we now go on to discuss.

After the work of Kadanoff [35], the scattering rates for polarons are calculated using Fermi’s golden rule, with eigenstates of Eq. (2),  $|\mathbf{K}_i, \mathbf{n}_i\rangle$  and  $|\mathbf{K}_f, \mathbf{n}_f\rangle$ , as the initial and final states. We restrict ourselves to the case in which the polaron is in its internal ground state both before and after the scattering event, i.e.,  $\mathbf{n}_f = \mathbf{n}_i = \mathbf{0}$ , which, in light of the discussion in

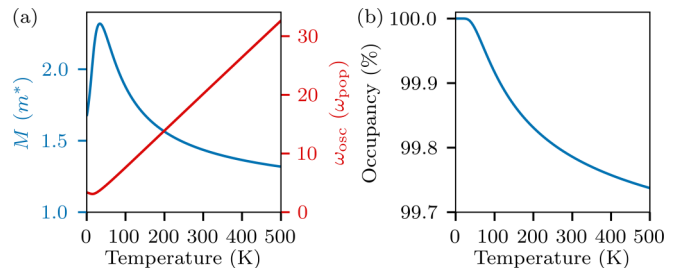


FIG. 1. (a) Temperature dependence of the mass  $M$  (in units of  $m^*$ , the bare band electron effective mass) and oscillator frequency  $\omega_{\text{osc}}$  (in units of  $\omega_{\text{pop}}$ , the effective polar optical phonon frequency) of the large electron polaron in MAPbI<sub>3</sub>. Both quantities were calculated using the material parameters compiled in Table I. (b) Temperature dependence of the occupancy of the internal harmonic oscillator ground state of the large electron polaron in MAPbI<sub>3</sub>.

the previous paragraph, we expect to be a valid approximation close to equilibrium.

The scattering rates  $S(\mathbf{K}_i \rightarrow \mathbf{K}_f)$  are therefore calculated according to the following general expression:

$$S(\mathbf{K}_i \rightarrow \mathbf{K}_f) = \frac{2\pi}{\hbar} |\langle \mathbf{K}_f, \mathbf{0} | H_{\text{pert}} | \mathbf{K}_i, \mathbf{0} \rangle|^2 \times \delta(E_{\mathbf{K}_f, \mathbf{0}} - E_{\mathbf{K}_i, \mathbf{0}} - \Delta E). \quad (3)$$

In Equation (3),  $H_{\text{pert}}$  is a time-dependent perturbing Hamiltonian, the forms of which are well known for the main scattering mechanisms in polar semiconductors, namely acoustic and polar optical phonons, and ionized impurities [38]. The magnitude of  $\Delta E$  in Eq. (3) depends on the scattering mechanism; for (quasi)elastic scattering, such as that due to acoustic phonons and ionized impurities,  $\Delta E = 0$ , while for polar optical phonon scattering,  $\Delta E = \hbar\omega_{\text{pop}}$ .

The derivations of the scattering rates are provided in the Supplemental Material [39], and the resulting forms compared with the corresponding rates for bare band carriers. In short, the differences between the scattering rates for polarons and those for band electrons amount to replacing  $\mathbf{k}$  in the band-electron expressions with  $\mathbf{K}$  and then multiplying by  $\exp(-\hbar m_{\text{red}} |\mathbf{K}_f - \mathbf{K}_i|^2 / 2(m^*)^2 \omega_{\text{osc}})$ , where  $m_{\text{red}} = m^* m_c / M$  is the reduced mass of the polaron. As previously noted for the case of polar optical phonon scattering [35,37], the exponential factor should act to suppress large changes in momentum, ostensibly supporting the hypothesis that polarons are protected from scattering in comparison to their band carrier counterparts. We begin investigating the validity of this hypothesis by examining the *total* scattering rates for each mechanism as functions of the particle's wave vector before scattering, which are calculated by integrating over all possible final states:

$$W(\mathbf{K}_i) = \int d^3 \mathbf{K}_f S(\mathbf{K}_i \rightarrow \mathbf{K}_f). \quad (4)$$

Total scattering rates for electron polarons in MAPbI<sub>3</sub> are plotted in Fig. 2 at 100 and 300 K; to enable a direct comparison with the analogous rates for band electrons, also plotted in Fig. 2, the rates are plotted as functions of the initial kinetic energy of the particle. For scattering due to ionized impurities, a density of such defects of  $10^{16} \text{ cm}^{-3}$  is assumed, which is towards the upper end of the range of values measured in polycrystalline LHP solar cells [18,47,48].

Of the mechanisms considered, the acoustic phonon scattering rate is the most significantly affected by polaron formation, while the effects on polar optical and impurity scattering rates are essentially negligible. In all cases, the differences between scattering rates for the bare band electron and the electron polaron are reduced at 300 K with respect to 100 K. We also note that polar optical phonon scattering is dominant for both band electrons and electron polarons, in contrast to assumptions made in a previous study [49].

In order to understand these results, we must examine the probability distributions of final states arising from a scattering event due to a given mechanism. Following a scattering event, a particle's *final* wave vector  $\mathbf{K}_f$  can be fully described by its spherical coordinates in a reference frame defined by its *initial* wave vector  $\mathbf{K}_i$ . The magnitude of  $\mathbf{K}_f$  is determined by the delta function in Eq. (3), so that the relevant function is

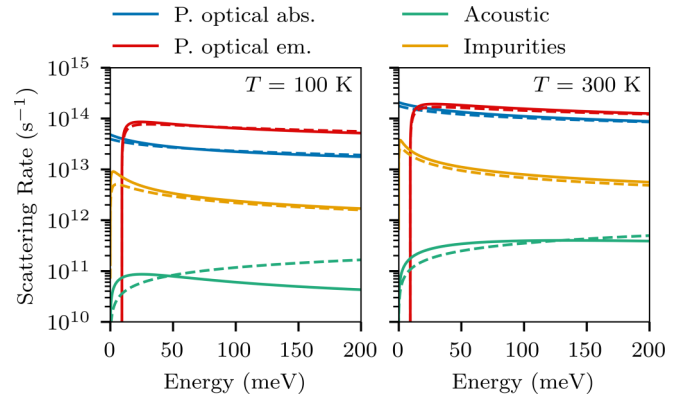


FIG. 2. Total scattering rates of large electron polarons (solid lines) and bare band electrons (dashed lines) in MAPbI<sub>3</sub>, at 100 and 300 K. Total (i.e., integrated over all final states) scattering rates due to polar optical phonon absorption and emission (P. optical abs. and em, respectively), acoustic phonons, and ionized impurities are shown. The rates are calculated using the material parameters compiled in Table I and the polaron mass  $M$  for the relevant temperature.

the probability density per unit solid angle of  $\mathbf{K}_f$  being at an angle  $\theta$  to  $\mathbf{K}_i$  following a scattering event:

$$S(\mathbf{K}_i, \theta) = \frac{\int d|\mathbf{K}_f| |\mathbf{K}_f|^2 S(\mathbf{K}_i \rightarrow \mathbf{K}_f)}{W(\mathbf{K}_i)}. \quad (5)$$

Note that the distribution of the azimuthal angle is constant due to the cylindrical symmetry of the reference frame (assuming isotropy of the underlying material, as we do here); therefore, only the dependence on the magnitude of the initial wave vector, and the (polar) angle between the final and initial wave vectors, need be considered.

The final state distributions at 100 and 300 K for both bare band electrons and polarons are plotted in Fig. 3 as functions of the polar angle  $\theta$  and the initial kinetic energy, which is used as the radial coordinate rather than the magnitude of the initial wave vector in order to facilitate comparison. In accordance with the total scattering rates plotted in Fig. 2, the most strongly affected distribution is that of acoustic phonon scattering, which is isotropic in the band electron case but exhibits the expected suppression of large changes in momentum in the polaron case. However, the impurity and polar optical phonon distributions are already strongly forward scattering for band electrons, so that the effects of the suppression of large changes in momentum in the polaron case are minor. Thus, although the concept of charge carriers being protected from scattering does survive some scrutiny, the effects appear to be non-negligible only in the case of acoustic phonon scattering at low temperatures. Furthermore, we expect their influence to be marginal in MAPbI<sub>3</sub>, since polar optical phonons remain the dominant cause of scattering.

Finally, as the simplest example of a measurable quantity that depends on scattering, we consider polaronic effects on the mobility of charge carriers in MAPbI<sub>3</sub>, at temperatures in the range of 50–500 K. The temperature dependence of the mobility has been measured experimentally using a variety of techniques, and despite a relatively large spread in absolute values, a  $\sim T^{-1.5}$  dependence has been consistently observed [50–53]. According to textbook semiconductor theory, a  $T^{-1.5}$

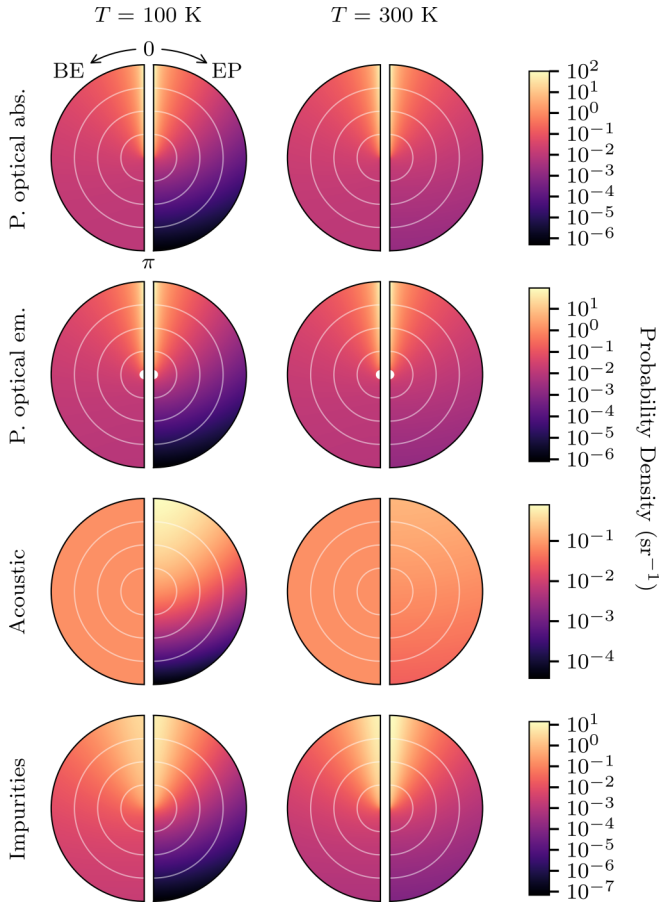


FIG. 3. Probability densities, per unit solid angle, of particle states after scattering in MAPbI<sub>3</sub> at 100 K and 300 K, as a function of the initial kinetic energy (in eV, radial coordinate) and the angle between the initial and final wave vectors (in radians, polar coordinate). The distributions for bare band electrons (BE) and large electron polarons (EP) are plotted on the left and right halves of each polar plot. The contours delineate divisions of 50 meV. The probabilities are calculated using the material parameters compiled in Table I and the polaron mass  $M$  for the relevant temperature.

dependence is indicative of acoustic phonons being the dominant cause of carrier scattering, but the values of mobility around room temperature calculated under that assumption are significantly greater than those observed [26,54]. On the other hand, if polar optical phonon scattering is assumed to be dominant, which is usually the case in polar semiconductors such as MAPbI<sub>3</sub>, the calculated room temperature mobilities are of the correct order of magnitude, but the temperature dependence approaches  $T^{-0.5}$  in the high temperature limit. The formation of large polarons has been proposed as one possible explanation for this apparently anomalous behavior [4,26,49].

We modelled polaron transport under the influence of an electric field using an augmented form of Kadanoff's semiclassical Boltzmann transport equation [35,37]. For an ensemble of electron polarons subject to a constant electric field  $\mathbf{E}$  in an otherwise homogeneous system (such as the bulk of a semiconductor, as considered here), the Boltzmann

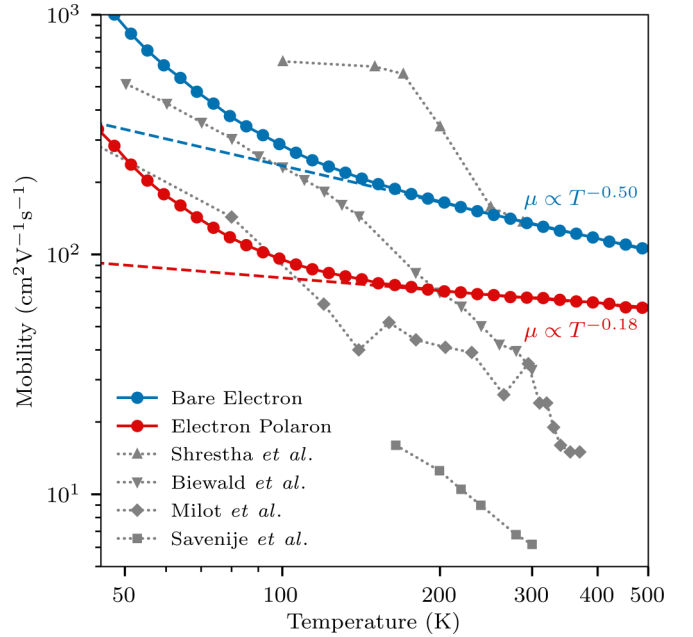


FIG. 4. Temperature dependent mobilities of bare band electrons and large electron polarons in MAPbI<sub>3</sub> (blue and red circles, respectively), calculated from steady state solutions to Boltzmann transport equations obtained using the ensemble Monte Carlo method, the material parameters compiled in Table I, and the polaron mass  $M$  for the relevant temperature. Experimental data from the literature are also shown: squares from Ref. [50], diamonds from Ref. [51], upward triangles from Ref. [52], and downward triangles from Ref. [53]. Lines between data points are plotted as guides to the eye only. Dashed lines are fits to the theoretical data for temperatures above 200 K.

transport equation reads

$$\frac{\partial f}{\partial t} - \frac{e}{\hbar} \mathbf{E} \cdot \frac{\partial f}{\partial \mathbf{K}} = \left( \frac{\partial f}{\partial t} \right)_{\text{pop}} + \left( \frac{\partial f}{\partial t} \right)_{\text{aco}} + \left( \frac{\partial f}{\partial t} \right)_{\text{imp}}, \quad (6)$$

where  $f(\mathbf{K}, t)$  is the one-particle distribution function. The three terms on the right hand side of Equation (6) represent the change in the distribution function due to each of the three scattering mechanisms considered above, namely polar optical phonons (pop), acoustic phonons (aco), and ionized impurities (imp); it is the final two of the three terms that are additional to Kadanoff's Boltzmann transport equation for polarons [35].

Essentially exact steady state solutions to Eq. (6) were obtained using the ensemble Monte Carlo method [38,55]; further details of the calculations can be found in the Supplemental Material [39]. The magnitude of the drift velocity  $\mathbf{v}_d$  was then determined from the ensemble average wave vector  $\overline{\mathbf{K}}$ , and the mobility  $\mu$  calculated according to

$$|\mathbf{v}_d| = \frac{\hbar |\overline{\mathbf{K}}|}{M} = \mu |\mathbf{E}|, \quad (7)$$

where  $M$  is the (temperature dependent) polaron mass. Analogous calculations were also carried out for bare band electrons, using the appropriate mass and scattering rates.

The calculated mobilities for large electron polarons and bare band electrons are plotted in Fig. 4, along with data

from several experimental studies of charge carrier mobility in MAPbI<sub>3</sub> for reference. For bare band electrons, fitting a power law to the theoretical data points for temperatures above 200 K recovers the expected  $T^{-0.50}$  dependence, with a value of  $\sim 130 \text{ cm}^2 \text{ V}^{-1} \text{ s}^{-1}$  at room temperature. Turning to the data for polarons, we see that the mobility at room temperature is reduced by almost a factor of 2 to  $\sim 70 \text{ cm}^2 \text{ V}^{-1} \text{ s}^{-1}$ , but more significantly, the temperature dependence of the mobility extracted for values above 200 K gives  $T^{-0.18}$ , which is further removed from the experimentally observed  $\sim T^{-1.5}$  dependence.

Several other possible microscopic mechanisms have been proposed as possible explanations for the observed temperature dependence of the mobility, namely (i) the enhancement of acoustic phonon scattering and suppression of polar optical phonon scattering due to Rashba splitting in the electronic band structure [56], (ii) vibrational anharmonicity and non-linear electron–phonon coupling [57], (iii) the presence of multiple low energy optical phonon modes [58], and (iv) microstructural disorder [59]. While our results indicate that polaronic effects alone do not provide an explanation for the apparently anomalous temperature dependence of carrier mobilities in MAPbI<sub>3</sub>, that does not necessarily preclude their playing a role in a quantitative theory of carrier dynamics in LHPs in which one or more of the effects listed above, or indeed, others which have not yet been considered, are included.

In conclusion, we have presented an analysis of the effects of large polaron formation in MAPbI<sub>3</sub> on carrier scattering and mobilities, by direct comparison of bare band electrons with large electron polarons on an equal theoretical footing. Our results show that, of the three mechanisms considered here, scattering of polarons due to acoustic phonons is the most significantly different from that of bare band carriers,

with the final state distribution exhibiting a striking change from an isotropic to an anisotropic one upon polaronic effects being taken into account. In contrast, the rates and final state distributions for scattering by polar optical phonons and ionized impurities, both of which are significantly stronger sources of scattering than acoustic phonons, are not significantly affected by polaron formation. We also found that the polaron mobility exhibits a smaller negative exponent for the temperature dependence than band electron mobility ( $T^{-0.18}$  vs  $T^{-0.50}$ ) in the high temperature limit, which suggests that other possible explanations should be considered for the  $\sim T^{-1.5}$  dependence of carrier mobility in MAPbI<sub>3</sub> observed in experiments. The results for holes in MAPbI<sub>3</sub>, and electrons and holes in MAPbBr<sub>3</sub> and CsPbI<sub>3</sub>, which are given in the Supplemental Material [39], are qualitatively similar and indicate that our conclusions apply generally to LHPs.

Finally, while our study provides evidence challenging the growing consensus that polaronic effects play a central role in understanding the optoelectronic properties of this important class of material, quantitative investigations of other critical aspects of charge-carrier dynamics, such as trapping and recombination, are required before a definitive conclusion as to the overall significance of polaronic effects can be reached.

This work was funded by the United Kingdom’s Engineering and Physical Sciences Research Council (EPSRC) through the Centre for Doctoral Training in New and Sustainable Photovoltaics (Grant Reference: EP/L01551X/1), and by the European Commission through the Horizon 2020 Framework Programme for Research and Innovation, Energy Oriented Centre of Excellence (EoCoE-II) project (Grant Agreement ID: 824158). We thank Prof. L. M. Peter for reading and commenting on an earlier draft of the Letter.

- 
- [1] A. K. Jena, A. Kulkarni, and T. Miyasaka, *Chem. Rev.* **119**, 3036 (2019).
- [2] D. A. Egger, A. Bera, D. Cahen, G. Hodes, T. Kirchartz, L. Kronik, R. Lovrincic, A. M. Rappe, D. R. Reichman, and O. Yaffe, *Adv. Mater.* **30**, 1800691 (2018).
- [3] L. M. Herz, *J. Phys. Chem. Lett.* **9**, 6853 (2018).
- [4] X. Zhu and V. Podzorov, *J. Phys. Chem. Lett.* **6**, 4758 (2015).
- [5] K. Miyata, T. L. Atallah, and X.-Y. Zhu, *Sci. Adv.* **3**, e1701469 (2017).
- [6] C. Wolf, H. Cho, Y.-H. Kim, and T.-W. Lee, *ChemSusChem* **10**, 3705 (2017).
- [7] D. Ghosh, E. Welch, A. J. Neukirch, A. Zakhidov, and S. Tretiak, *J. Phys. Chem. Lett.* **11**, 3271 (2020).
- [8] A. M. Soufiani, F. Huang, P. Reece, R. Sheng, A. Ho-Baillie, and M. A. Green, *Appl. Phys. Lett.* **107**, 231902 (2015).
- [9] E. Menéndez-Proupin, C. L. Beltrán Ríos, and P. Wahnón, *Phys. Status Solidi RRL* **9**, 559 (2015).
- [10] M. Bokdam, T. Sander, A. Stroppa, S. Picozzi, D. Sarma, C. Franchini, and G. Kresse, *Sci. Rep.* **6**, 28618 (2016).
- [11] D. B. Straus, S. Hurtado Parra, N. Iotov, J. Gebhardt, A. M. Rappe, J. E. Subotnik, J. M. Kikkawa, and C. R. Kagan, *J. Am. Chem. Soc.* **138**, 13798 (2016).
- [12] D. Niesner, H. Zhu, K. Miyata, P. P. Joshi, T. J. Evans, B. J. Kudisch, M. T. Trinh, M. Marks, and X.-Y. Zhu, *J. Am. Chem. Soc.* **138**, 15717 (2016).
- [13] H. Zhu, K. Miyata, Y. Fu, J. Wang, P. P. Joshi, D. Niesner, K. W. Williams, S. Jin, and X.-Y. Zhu, *Science* **353**, 1409 (2016).
- [14] J. M. Frost, L. D. Whalley, and A. Walsh, *ACS Energy Lett.* **2**, 2647 (2017).
- [15] Z. Guo, Y. Wan, M. Yang, J. Snaider, K. Zhu, and L. Huang, *Science* **356**, 59 (2017).
- [16] T. J. Evans, K. Miyata, P. P. Joshi, S. Maehrlein, F. Liu, and X.-Y. Zhu, *J. Phys. Chem. C* **122**, 13724 (2018).
- [17] P. P. Joshi, S. F. Maehrlein, and X. Zhu, *Adv. Mater.* **31**, 1803054 (2019).
- [18] Y. Chen, H. Yi, X. Wu, R. Haroldson, Y. Gartstein, Y. Rodionov, K. Tikhonov, A. Zakhidov, X.-Y. Zhu, and V. Podzorov, *Nat. Commun.* **7**, 12253 (2016).
- [19] T. Ivanovska, C. Dionigi, E. Mosconi, F. De Angelis, F. Liscio, V. Morandi, and G. Ruani, *J. Phys. Chem. Lett.* **8**, 3081 (2017).
- [20] F. Ambrosio, J. Wiktor, F. De Angelis, and A. Pasquarello, *Energy Environ. Sci.* **11**, 101 (2018).
- [21] J. He, M. Guo, and R. Long, *J. Phys. Chem. Lett.* **9**, 3021 (2018).

- [22] K. T. Munson, E. R. Kennehan, G. S. Doucette, and J. B. Asbury, *Chem.* **4**, 2826 (2018).
- [23] J. Wiktor, F. Ambrosio, and A. Pasquarello, *J. Mater. Chem. A* **6**, 16863 (2018).
- [24] K. T. Munson, G. S. Doucette, E. R. Kennehan, J. R. Swartzfager, and J. B. Asbury, *J. Phys. Chem. C* **123**, 7061 (2019).
- [25] M. Sendner, P. K. Nayak, D. A. Egger, S. Beck, C. Müller, B. Epding, W. Kowalsky, L. Kronik, H. J. Snaith, A. Pucci *et al.*, *Mater. Horiz.* **3**, 613 (2016).
- [26] P.-A. Mante, C. C. Stoumpos, M. G. Kanatzidis, and A. Yartsev, *Nat. Commun.* **8**, 14398 (2017).
- [27] A. Shluger and A. Stoneham, *J. Phys.: Condens. Matter* **5**, 3049 (1993).
- [28] H. Oberhofer, K. Reuter, and J. Blumberger, *Chem. Rev.* **117**, 10319 (2017).
- [29] L. M. Herz, *ACS Energy Lett.* **2**, 1539 (2017).
- [30] J. M. Frost, *Phys. Rev. B* **96**, 195202 (2017).
- [31] M. Schlipf, S. Poncé, and F. Giustino, *Phys. Rev. Lett.* **121**, 086402 (2018).
- [32] M. Puppini, S. Polishchuk, N. Colonna, A. Crepaldi, D. N. Dirin, O. Nazarenko, R. De Gennaro, G. Gatti, S. Roth, T. Barillot, L. Poletto, R. P. Xian, L. Rettig, M. Wolf, R. Ernstorfer, M. V. Kovalenko, N. Marzari, M. Grioni, and M. Chergui, *Phys. Rev. Lett.* **124**, 206402 (2020).
- [33] R. P. Feynman, *Phys. Rev.* **97**, 660 (1955).
- [34] Y. Osaka, *Prog. Theor. Phys.* **22**, 437 (1959).
- [35] L. P. Kadanoff, *Phys. Rev.* **130**, 1364 (1963).
- [36] J. Devreese, [arXiv:1611.06122v5](https://arxiv.org/abs/1611.06122v5).
- [37] F. Peeters and J. Devreese, in *Solid State Physics* (Academic Press Inc., Orlando, 1984), Vol. 38, pp. 81–133.
- [38] C. Jacoboni and P. Lugli, *The Monte Carlo Method for Semiconductor Device Simulation* (Springer-Verlag, Vienna, 1989).
- [39] See Supplemental Material at <http://link.aps.org/supplemental/10.1103/PhysRevB.103.L220305> for results and material parameters for electrons and holes in MAPbI<sub>3</sub>, results and material parameters for electrons and holes in MAPbBr<sub>3</sub> and CsPbI<sub>3</sub>, further details of the computational method, derivations of the rates of scattering of large polarons by acoustic phonons, polar optical phonons, and ionized impurities, and additional references; E. Mosconi, P. Umari, and F. De Angelis, *J. Mater. Chem. A* **3**, 9208 (2015); D. Zhao, J. M. Skelton, H. Hu, C. La-o-vorakiat, J.-X. Zhu, R. A. Marcus, M.-E. Michel-Beyerle, Y. M. Lam, A. Walsh, and E. E. Chia, *Appl. Phys. Lett.* **111**, 201903 (2017); D. Howarth and E. H. Sondheimer, *Proc. R. Soc. Lond. A* **219**, 53 (1953); F. J. Blatt, in *Solid State Physics* (Academic Press Inc., New York, 1957), Vol. 4, pp. 199–366; N. Ashcroft and N. Mermin, *Solid State Physics*, (Saunders College Publishing, New York, 1976); L. Kadanoff and M. Revzen, *Il Nuovo Cimento* **33**, 397 (1964); Y. Osaka, *J. Phys. Soc. Jpn.* **21**, 423 (1966); **35**, 381 (1973); K. Okamoto and S. Takeda, *ibid.* **37**, 333 (1974); R. W. Hockney and J. W. Eastwood, *Computer Simulation Using Particles* (CRC Press, Boca Raton, 1988); K. Tomizawa, *Numerical Simulation of Submicron Semiconductor Devices* (Artech House, Boston, 1993); J. D. Hunter, *Comput. Sci. Eng.* **9**, 90 (2007); C. Jacoboni, *Theory of Electron Transport in Semiconductors: A Pathway from Elementary Physics to Nonequilibrium Green Functions* (Springer-Verlag, Berlin, Heidelberg, 2010).
- [40] J.-H. Lee, Z. Deng, N. C. Bristowe, P. D. Bristowe, and A. K. Cheetham, *J. Mater. Chem. C* **6**, 12252 (2018).
- [41] F. Brivio, K. T. Butler, A. Walsh, and M. Van Schilfgaarde, *Phys. Rev. B* **89**, 155204 (2014).
- [42] F. Brivio, A. B. Walker, and A. Walsh, *APL Mater.* **1**, 042111 (2013).
- [43] T. Hahn, S. Klimin, J. Tempere, J. T. Devreese, and C. Franchini, *Phys. Rev. B* **97**, 134305 (2018).
- [44] W. H. Sio, C. Verdi, S. Poncé, and F. Giustino, *Phys. Rev. B* **99**, 235139 (2019).
- [45] W. H. Sio, C. Verdi, S. Poncé, and F. Giustino, *Phys. Rev. Lett.* **122**, 246403 (2019).
- [46] R. W. Hellwarth and I. Biaggio, *Phys. Rev. B* **60**, 299 (1999).
- [47] T. Leijtens, G. E. Eperon, A. J. Barker, G. Grancini, W. Zhang, J. M. Ball, A. R. S. Kandada, H. J. Snaith, and A. Petrozza, *Energy Environ. Sci.* **9**, 3472 (2016).
- [48] D. W. de Quilettes, S. M. Vorpahl, S. D. Stranks, H. Nagaoka, G. E. Eperon, M. E. Ziffer, H. J. Snaith, and D. S. Ginger, *Science* **348**, 683 (2015).
- [49] M. Zhang, X. Zhang, L.-Y. Huang, H.-Q. Lin, and G. Lu, *Phys. Rev. B* **96**, 195203 (2017).
- [50] T. J. Savenije, C. S. Ponseca Jr, L. Kunneman, M. Abdellah, K. Zheng, Y. Tian, Q. Zhu, S. E. Canton, I. G. Scheblykin, T. Pullerits *et al.*, *J. Phys. Chem. Lett.* **5**, 2189 (2014).
- [51] R. L. Milot, G. E. Eperon, H. J. Snaith, M. B. Johnston, and L. M. Herz, *Adv. Funct. Mater.* **25**, 6218 (2015).
- [52] S. Shrestha, G. J. Matt, A. Osvet, D. Niesner, R. Hock, and C. J. Brabec, *J. Phys. Chem. C* **122**, 5935 (2018).
- [53] A. Biewald, N. Giesbrecht, T. Bein, P. Docampo, A. Hartschuh, and R. Ciesielski, *ACS Appl. Mater. Interfaces* **11**, 20838 (2019).
- [54] T. Zhao, W. Shi, J. Xi, D. Wang, and Z. Shuai, *Sci. Rep.* **6**, 19968 (2016).
- [55] W. Fawcett, A. Boardman, and S. Swain, *J. Phys. Chem. Solids* **31**, 1963 (1970).
- [56] Z.-G. Yu, *J. Phys. Chem. Lett.* **7**, 3078 (2016).
- [57] M. Z. Mayers, L. Z. Tan, D. A. Egger, A. M. Rappe, and D. R. Reichman, *Nano Lett.* **18**, 8041 (2018).
- [58] S. Poncé, M. Schlipf, and F. Giustino, *ACS Energy Lett.* **4**, 456 (2019).
- [59] A. Lacroix, G. T. De Laissardière, P. Quémerais, J.-P. Julien, and D. Mayou, *Phys. Rev. Lett.* **124**, 196601 (2020).